Applied Mathematical Modelling 118 (2023) 818–831

Contents lists available at ScienceDirect

Applied Mathematical Modelling

journal homepage: www.elsevier.com/locate/apm

Incremental harmonic balance method for multi-harmonic solution of high-dimensional delay differential equations: Application to crossflow-induced nonlinear vibration of steam generator tubes

Pan Sun [a], Xielin Zhao [a], Xiaofei Yu [b], Qian Huang [b], Zhipeng Feng [b], Jinxiong Zhou [a,*]

[a] State Key Laboratory for Strength and Vibration of Mechanical Structures and School of Aerospace, Xi'an Jiaotong University, Xi'an 710049, People's Republic of China
[b] Key Laboratory of Nuclear Reactor System Design Technology, Nuclear Power Institute of China, Chengdu 610200, People's Republic of China

A R T I C L E I N F O

Article history:
Received 21 October 2022
Revised 8 February 2023
Accepted 13 February 2023
Available online 15 February 2023

Keywords:
Delay differential equation (DDEs)
Incremental harmonic balance (IHB) method
Flow-induced vibration (FIV)
Finite element method
Limit cycle

A B S T R A C T

Diverse science and engineering problems are governed by delay differential equations (DDE). Seeking periodic solutions of DDEs is crucial for many nonlinear dynamic systems. The incremental harmonic balance (IHB) method is an efficient semi-analytical approach for periodic solutions of DDE. Among various DDE systems, flow-induced vibration (FIV) of tube bundles with loose support is unique, in the sense that the added damping cancels out structural damping in the vicinity of critical velocity, making it extremely slow to retain a convergent solution if numerical integration (NI) is utilized. Despite the efforts of developing IHB for various mechanical vibration problems with time-delay, no attempt has been made to employ IHB to nonlinear FIV problems. Here we fill this blank by separately combining two spatial discretization strategies, i.e., discretization via linear vibration modes or via finite element method (FEM), with IHB to capture limit cycle solutions after the onset of instability. Within the range of gap velocity of interest, the IHB demonstrates excellent convergence by increasing harmonic terms, and good agreement is obtained between IHB results and the results by NI method. An 18 degree-of-freedom (DOF) nonlinear DDE system was readily dealt by integrating FEM and IHB, each DOF being approximated by three harmonics. This is the first attempt to employ IHB for multi-harmonic solution of high-dimensional FIV problems, which opens a door for solutions of other DDEs. All the codes used in this paper could be downloaded via: https://github.com/XJTU-Zhou-group/IHB.

1. Introduction

Many actual dynamic systems have the property of aftereffect, i.e, the evolution rate of these systems depends not only on the present, but also on the past history [1]. One particular type of systems is time-delay systems, whose governing

* Corresponding author.
E-mail address: jxzhouxx@mail.xjtu.edu.cn (J. Zhou).

https://doi.org/10.1016/j.apm.2023.02.018
0307-904X/

equations are delay differential equations (DDE). Processes and systems having aftereffect and governed by DDE include biology, chemistry, economics, mechanics, physics, physiology, population dynamics, as well as in engineering science [2–4]. In addition, actuators, sensors, communication and information technologies, field networks usually also introduce such delays and the systems are also dictated by DDEs [4].

Dynamics systems with DDEs may exhibit fruitful nonlinear phenomena, whereas the periodic solutions are regarded as the most important aspect of the nonlinear dynamics. DDEs are infinite-dimensional as opposed to finite-dimensional ordinary differential equations (ODE). Numerical methods have been developed to find solutions of DDE, and periodic solution is the first priority. In the community of nonlinear dynamics, approaches for periodic solutions of DDE include numerical integration (NI) method [5–8], harmonic balance (HB) method [9–11], incremental harmonic balance (IHB) method [12–15], perturbation and multiple scales method [16–20] shooting and collocation method [21–23]. DDEs are infinite-dimensional because their solutions are unique only when an initial function is specified on a time interval equal to the largest delay. Consequently, solutions of DDEs are more difficult than for ODEs. During the past decades, more efficient and reliable methods have been developed for DDEs. The monograph by Bellen and Zeunaro [3] includes various numerical methods for DDE. A DDE can be approximated by a set of ODEs and thus the well-developed numerical integration methods for ODEs could be used. However, to obtain an accurate approximation a high-dimensional system of ODEs is needed, and this leads to expensive numerical procedures [8]. A noticeable progress during the past decades is the combination of NI method or extended shooting method with continuation methods, resulting in numerical tools for bifurcation of DDE. Engelborghs and co-workers developed a numerical tool called DDEs-BIFTOOL for various DDEs [5,6]. Pieroux and Mandel [7] studied the bifurcation diagrams of the Lang-Kobayashi equation with cubic nonlinearity by using NI method. MacDonald [9] proposed to use HB method to Blaquiere equation, pinney's equation and the sunflower equation. Liu and Kalmár-Nagy [10] demonstrated the use of high-dimensional HB method for limit cycles of DDEs. They applied the method for machine tool vibration model, the sunflower model and a circadian rhythm model. Shakeri and Dehghan [16] presented a homotopy perturbation method to solve various DDEs. He [17] presented an analytical iteration method combined with homotopy perturbation method for periodic solutions and bifurcations of DDE. Chen and Xu [18] investigated the integral equation method and the multiple scales method for determining the amplitude equations of DDEs. Guillot et al. [11] extended the asymptotic numerical method combined with the HB method to the continuation of periodic orbits of DDE. The method was applied to various DDEs, from Van der Pol and Duffing oscillators to toy models of clarinet and saxophone. Wang and Hu [21] utilized multiple scales method and the shooting technique to probe bifurcations of second-order DDEs. Barton et al. [23] proposed a collocation scheme for periodic solutions for neutral DDEs. Maccari [19,20] used the asymptotic perturbation method to investigate the primary resonance of a Van der Pol oscillator under state feedback control with a time delay.

Among these various approaches, the perturbation method and the multiple scales method are analytical and therefore the most efficient approaches, but are limited to systems with weak nonlinearity. HB method is a classical semi-analytical method and is suitable for both weak and strong nonlinearities. HB can capture both stable and unstable solutions. The main drawback of HB method is it is very cumbersome for multi-harmonic analysis. If an approximation with more harmonic terms is needed, the whole formulation and derivations of HB should be reformulated again. Direct NI method is the most basic and fundamental way for DDEs. However, simple NI method can only give stable solutions, and extension is made to develop shooting method or numerical continuation method for the case where bost stable and unstable solutions and bifurcation are interested.

Research interests have flourished regarding extension of conventional HB method to IHB for efficient periodic solutions of DDEs. Wang et al. [12] derived a general formula of Jacobin matrix in IHB and applied the method for a SDOF delayed Van der Pol equation. Song and Zhu [13] applied IHB for elastic wave propagation in strongly nonlinear lattice. Wu et al. [24] investigated the periodic solutions of a harmonically excited Duffing oscillator with time-delay state feedback. Mitra et al. [14] employed the IHB method along with arc-length continuation method to study the response of a harmonically forced dry friction damped system under time-delayed state feedback control. Liu et al. [15] used IHB to study a nonlinear vehicle/driver closed-loop system with time delay.

Previous studies on use of IHB to DDEs are limited to low-dimensional toy models. Derivations and formulations of governing equations of practical applications involve more DOFs, more physical mechanisms and control factors and strong nonlinearity, resulting in nonlinear high-dimensional DDEs. To approximate the solutions of these DDEs accurately, a multi-harmonic approximation is inevitable. It is a plausible question whether IHB can handle this high-dimensional DDE more efficiently? We are concerned with the use of IHB for multi-harmonic analysis of high-dimensional DDE, which is of utmost importance for various engineering problems. Here we use the cross-flow induced vibration of tube bundles as an example and demonstrate the success and robustness of IHB for determining complicated limit cycle solutions of the system. FIV of tube bundles are ubiquitous fluid-structure interaction phenomena in the fields of steam generators, heat exchangers, fluid-conveying pipes and galloping of transmission lines. The reason for the appearance of time delay in this system is understood as the fact that the fluid surrounding the tubes does not æfeelg instantaneously the change in tube position. Instead, a time delay is required for the flow to react to the tube vibration, which was pointed out by Robert in 1966 [25]. Previously, this canonical FIV system with nonlinear support was studied by Paidoussis and Li [26] using NI method. Using direct NI method to obtain periodic solutions of the above high-dimensional DDEs is not the most economic means, because a long period of transient dynamics is unavoidable before a final limit cycle solution is approached. Moreover, a DDE is infinite-dimensional in principle in the sense that infinitely many initial conditions over a continuous range are required for NI method, and the accurate solution of the system can only be obtained by solving infinite-dimensional ODEs.

Lastly but not the least, the added damping cancels out structural damping in the vicinity of critical velocity of FIV systems, making it extremely slow to retain a convergent solution if NI is utilized. These issues associated with NI can be handled by the semi-analytical IHB method. We revisit this problem and propose to use IHB for this problem and provide the first reference on the use of IHB for high-dimensional FIV problems.

This paper is organized as follows. The IHB formulations for general multiple-DOF(MDOF) DDEs with multiple time delays are derived in Section 2, with an emphasis on the treatment of time delay in the context of IHB. We discuss two spatial discretization strategies combined with IHB for nonlinear FIV problems, i.e., discretization via vibration modes and via FEM, and highlight their difference. Numerical examples are presented in Section 3. We start with the simplest Van der Pol equation with time delay and then move to the nonlinear FIV problem with cubic nonlinearity. We then present the results by combining mode truncations and IHB and investigate the evolution of limit cycles under various gap velocities. We also perform a convergence study on the number of mode truncations on the solution errors of the system. The results by mode truncation and IHB is compared with the results by NI by using a Matlab routine DDE23 and good agreement is achieved. We finally demonstrate the results by FEM and IHB for an 18DOF FIV system. A multi-harmonic IHB analysis for such a high-dimensional DDE was carried out, and compared with NI results by using a home-made Newmark NI code. The Newmark NI code outperforms DDE23 in Matlab in particular for such high-dimensional DDEs. All the codes used in this paper could be downloaded via: https://github.com/XJTU-Zhou-group/IHB.

2. IHB formulations for MDOF DDE

2.1. IHB for general DDE

IHB method was firstly proposed by Lau and Cheung [27]. It has been successfully applied for various nonlinear vibrations without time delay [28–32]. We are trying to extending classical IHB to incorporate time delay for high-dimensional DDEs. We are concerned with a nonlinear DDE system with n DOF, which can be expressed in matrix form as

$$\bar{\mathbf{M}}\mathbf{q}'' + \bar{\mathbf{C}}\mathbf{q}' + \bar{\mathbf{K}}\mathbf{q} + \bar{\mathbf{E}}\mathbf{q}_d + \bar{\mathbf{f}} = 0 \tag{1}$$

where

$$\begin{aligned}
&\mathbf{q} = \{q_1, q_2, \ldots, q_n\}^T,\\
&\mathbf{q}_d = \{q_1(t-t_{d1}), q_2(t-t_{d2}), \ldots, q_n(t-t_{dn})\}^T,\\
&\bar{\mathbf{f}} = \left\{\bar{f}_1, \bar{f}_2, \ldots, \bar{f}_n\right\}^T,\\
&\bar{f}_i = \bar{f}_i(q_1, q_2, \ldots, q_n, \dot{q}_1, \dot{q}_2, \ldots, \dot{q}_n, \omega, \lambda, t) \qquad i = 1, 2, \ldots, n.
\end{aligned}$$

The matrices $\bar{\mathbf{M}}$, $\bar{\mathbf{C}}$, $\bar{\mathbf{K}}$ are conventional mass, damping and stiffness matrices, respectively. $\mathbf{q}_d$ is the vector contains time delay. $\bar{\mathbf{E}}$ is a coefficient matrix and the product of $\bar{\mathbf{E}}$ with $\mathbf{q}_d$ gives the time-delay loading. $\bar{\mathbf{f}}$ is the load vector containing all sources of loads without time-delay. The primes represent derivatives with respect to time t. $t_{d1}, t_{d2}, \ldots, t_{dn}$ are n time delays, and λ is an arbitrary physical parameter of the system. Let ω be the frequency of the system, and introduce dimensionless time $\tau = \omega t$ and dimensionless time delay $\tau_{di} = \omega t_{di} (i = 1, 2, \ldots, n)$, Eq. (1) can be rewritten into the following form

$$\omega^2\bar{\mathbf{M}}\ddot{\mathbf{q}} + \omega\bar{\mathbf{C}}\dot{\mathbf{q}} + \bar{\mathbf{K}}\mathbf{q} + \bar{\mathbf{E}}\mathbf{q}_d + \bar{\mathbf{f}}(\mathbf{q}, \dot{\mathbf{q}}, \omega, \lambda, \tau) = 0 \tag{2}$$

Here, the dots represent derivatives with respect to dimensionless time τ.

Suppose we have already found a solution of the system, denoted by $\mathbf{q}_0$, $\mathbf{q}_{d0}$, ω_0 and λ_0, a new solution can be achieved by perturbing the known solution by the following increments

$$\begin{aligned}
&\mathbf{q} = \mathbf{q}_0 + \Delta\mathbf{q}\\
&\mathbf{q}_d = \mathbf{q}_{d0} + \Delta\mathbf{q}_d\\
&\omega = \omega_0 + \Delta\omega\\
&\lambda = \lambda_0 + \Delta\lambda
\end{aligned} \tag{3}$$

in which

$$\begin{aligned}
&\mathbf{q}_0 = \{q_{10}, q_{20}, \ldots, q_{n0}\}^T,\\
&\Delta\mathbf{q} = \{\Delta q_1, \Delta q_2, \ldots, \Delta q_n\}^T,\\
&\mathbf{q}_{d0} = \{q_{10}(\tau-\tau_{d1}), q_{20}(\tau-\tau_{d2}), \ldots, q_{n0}(\tau-\tau_{dn})\}^T,\\
&\Delta\mathbf{q}_d = \{\Delta q_1(\tau-\tau_{d1}), \Delta q_2(\tau-\tau_{d2}), \ldots, \Delta q_n(\tau-\tau_{dn})\}^T.
\end{aligned}$$

Substituting Eq. (3) into Eq. (2), and neglecting high-order terms, the linearized incremental equation is obtained as follows:

$$\omega_0{}^2\bar{\mathbf{M}}\Delta\ddot{\mathbf{q}} + (\omega_0\bar{\mathbf{C}} + \bar{\mathbf{C}}_N)\Delta\dot{\mathbf{q}} + (\bar{\mathbf{K}} + \bar{\mathbf{K}}_N)\Delta\mathbf{q} + \bar{\mathbf{E}}\Delta\mathbf{q}_d = \bar{\mathbf{R}} - (2\omega_0\bar{\mathbf{M}}\ddot{\mathbf{q}}_0 + \bar{\mathbf{C}}\dot{\mathbf{q}}_0 + \bar{\mathbf{Q}})\Delta\omega - \bar{\mathbf{P}}\Delta\lambda \tag{4}$$

where

$$\bar{\mathbf{K}}_N = \left(\frac{\partial \bar{\mathbf{f}}}{\partial \mathbf{q}}\right)_0, \bar{\mathbf{C}}_N = \left(\frac{\partial \bar{\mathbf{f}}}{\partial \dot{\mathbf{q}}}\right)_0, \bar{\mathbf{Q}} = \left(\frac{\partial \bar{\mathbf{f}}}{\partial \omega}\right)_0, \bar{\mathbf{P}} = \left(\frac{\partial \bar{\mathbf{f}}}{\partial \lambda}\right)_0,$$
$$\bar{\mathbf{R}} = -(\omega_0^2 \bar{\mathbf{M}}\ddot{\mathbf{q}}_0 + \omega_0 \bar{\mathbf{C}}\dot{\mathbf{q}}_0 + \bar{\mathbf{K}}\mathbf{q}_0 + \bar{\mathbf{E}}\mathbf{q}_{d0} + \bar{\mathbf{f}}_0).$$

$\mathbf{R}$ is the residual vector which vanishes when the target solution is sought. We are concerned with odd systems in this paper, thus the solution and its increment can be expressed by the following harmonic series:

$$q_{j0} = \sum_{k=1}^{N} \left[a_{jk}\cos(2k-1)\tau + b_{jk}\sin(2k-1)\tau\right] = \mathbf{C}\mathbf{A}_j \tag{5}$$

$$\Delta q_j = \sum_{k=1}^{N} \left[\Delta a_{jk}\cos(2k-1)\tau + \Delta b_{jk}\sin(2k-1)\tau\right] = \mathbf{C}\Delta\mathbf{A}_j \tag{6}$$

where

$$\mathbf{C} = [\cos\tau, \cos 3\tau, \ldots, \cos(2N-1)\tau, \sin\tau, \sin 3\tau, \ldots, \sin(2N-1)\tau],$$
$$\mathbf{A}_j = \left[a_{j1}, a_{j2}, \ldots, a_{jN}, b_{j1}, b_{j2}, \ldots, b_{jN}\right]^T,$$
$$\Delta\mathbf{A}_j = \left[\Delta a_{j1}, \Delta a_{j2}, \ldots, \Delta a_{jN}, \Delta b_{j1}, \Delta b_{j2}, \ldots, \Delta b_{jN}\right]^T.$$

N is the number of harmonic terms used in IHB approximation.

In employing IHB for DDE, the handle of time delay is crucial and is detailed here. The counterpart equations to Eqs. (5) and (6) can be derived by using the sum and difference formulas of trigonometric functions as

$$q_{j0}\left(\tau - \tau_{dj}\right) = \sum_{k=1}^{N} \left[a_{jk}\cos(2k-1)\left(\tau - \tau_{dj}\right) + b_{jk}\sin(2k-1)\left(\tau - \tau_{dj}\right)\right] = \mathbf{C}\boldsymbol{\Gamma}_j\mathbf{A}_j \tag{7}$$

$$\Delta q_j\left(\tau - \tau_{dj}\right) = \sum_{k=1}^{N} \left[\Delta a_{jk}\cos(2k-1)\left(\tau - \tau_{dj}\right) + \Delta b_{jk}\sin(2k-1)\left(\tau - \tau_{dj}\right)\right] = \mathbf{C}\boldsymbol{\Gamma}_j\Delta\mathbf{A}_j \tag{8}$$

where

$$\boldsymbol{\Gamma}_j = \begin{bmatrix} \cos\tau_{dj} & 0 & \cdots & 0 & -\sin\tau_{dj} & 0 & \cdots & 0 \\ 0 & \cos 3\tau_{dj} & \cdots & 0 & 0 & -\sin 3\tau_{dj} & \cdots & 0 \\ \vdots & \vdots & \ddots & \vdots & \vdots & \vdots & \ddots & \vdots \\ 0 & 0 & \cdots & \cos(2N-1)\tau_{dj} & 0 & 0 & 0 & -\sin(2N-1)\tau_{dj} \\ \sin\tau_{dj} & 0 & \cdots & 0 & \cos\tau_{dj} & 0 & \cdots & 0 \\ 0 & \sin 3\tau_{dj} & \cdots & 0 & 0 & \cos 3\tau_{dj} & \cdots & 0 \\ \vdots & \vdots & \ddots & 0 & \vdots & \vdots & \ddots & \vdots \\ 0 & 0 & \cdots & \sin(2N-1)\tau_{dj} & 0 & 0 & \cdots & \cos(2N-1)\tau_{dj} \end{bmatrix} \tag{9}$$

Thus matrices $\boldsymbol{\Gamma}_j$ in Eq. (9) account for the effect of time delay on the harmonic balance approximation of a solution and its increment. By assembling all components, the vectors of a known solution and its increment are given as

$$\begin{aligned} \mathbf{q}_0 &= \mathbf{S}\mathbf{A} \\ \Delta\mathbf{q} &= \mathbf{S}\Delta\mathbf{A} \\ \mathbf{q}_{d0} &= \mathbf{S}\boldsymbol{\Gamma}\mathbf{A} \\ \Delta\mathbf{q}_d &= \mathbf{S}\boldsymbol{\Gamma}\Delta\mathbf{A} \end{aligned} \tag{10}$$

where $\mathbf{S}$, $\mathbf{A}$ and $\Delta\mathbf{A}$, $\boldsymbol{\Gamma}$ are given as follows:

$$\mathbf{A} = [\mathbf{A}_1, \mathbf{A}_2, \ldots \mathbf{A}_n]^T, \ \Delta\mathbf{A} = [\Delta\mathbf{A}_1, \Delta\mathbf{A}_2, \ldots \Delta\mathbf{A}_n]^T, \ \mathbf{S} = \begin{bmatrix} \mathbf{C} & & & \\ & \mathbf{C} & & \\ & & \ddots & \\ & & & \mathbf{C} \end{bmatrix}, \ \boldsymbol{\Gamma} = \begin{bmatrix} \boldsymbol{\Gamma}_1 & & & \\ & \boldsymbol{\Gamma}_2 & & \\ & & \ddots & \\ & & & \boldsymbol{\Gamma}_n \end{bmatrix} \tag{11}$$

Equation (4) are ODEs, which can be converted into algebraic equations by applying the Galerkin procedure. The Galerkin procedure gives

$$\begin{aligned} &\int_0^{2\pi} \delta(\Delta\mathbf{q})^T\left[\omega_0^2\overline{\mathbf{M}}\Delta\ddot{\mathbf{q}} + \left(\omega_0\overline{\mathbf{C}} + \overline{\mathbf{C}}_N\right)\Delta\dot{\mathbf{q}} + \left(\overline{\mathbf{K}} + \overline{\mathbf{K}}_N\right)\Delta\mathbf{q} + \overline{\mathbf{E}}\Delta\mathbf{q}_d\right]d\tau \\ &\quad = \int_0^{2\pi} \delta(\Delta\mathbf{q})^T\left[\overline{\mathbf{R}} - \left(2\omega_0\overline{\mathbf{M}}\ddot{\mathbf{q}}_0 + \overline{\mathbf{C}}\dot{\mathbf{q}}_0 + \overline{\mathbf{Q}}\right)\Delta\omega - \overline{\mathbf{P}}\Delta\lambda\right]d\tau \end{aligned} \tag{12}$$

where $\delta(\Delta\mathbf{q})$ is an arbitrary test function and approximated in the same way as Eq. (10) using the same basic harmonic functions. Performing integrals on both hands of Eq. (12) results in the following linearized algebraic equations

$$\mathbf{K}_{mc}\Delta\mathbf{A} = \mathbf{R} - \mathbf{R}_{mc}\Delta\omega - \mathbf{P}\Delta\lambda \tag{13}$$

in which

$$\begin{aligned}
&\mathbf{K}_{mc} = {\omega_0}^2\mathbf{M}+\omega_0\mathbf{C} + \mathbf{C}_N+\mathbf{K} + \mathbf{K}_N+\mathbf{E}\\
&\mathbf{R} = -(\omega_0^2\mathbf{M}+\omega_0\mathbf{C} + \mathbf{K} + \mathbf{E})\mathbf{A} - \mathbf{f}_0\\
&\mathbf{R}_{mc} = (2\omega_0\mathbf{M} + \mathbf{C})\mathbf{A}+\mathbf{Q}\\
&\mathbf{M} = \int_0^{2\pi}\mathbf{S}^T\overline{\mathbf{M}}\dot{\mathbf{S}}d\tau,\quad \mathbf{C} = \int_0^{2\pi}\mathbf{S}^T\overline{\mathbf{C}}\dot{\mathbf{S}}d\tau,\quad \mathbf{C}_N = \int_0^{2\pi}\mathbf{S}^T\overline{\mathbf{C}}_N\dot{\mathbf{S}}d\tau,\quad \mathbf{K} = \int_0^{2\pi}\mathbf{S}^T\overline{\mathbf{K}}\mathbf{S}d\tau\\
&\mathbf{K}_N = \int_0^{2\pi}\mathbf{S}^T\overline{\mathbf{K}}_N\mathbf{S}d\tau,\quad \mathbf{E} = \int_0^{2\pi}\mathbf{S}^T\overline{\mathbf{E}}\mathbf{S}\boldsymbol{\Gamma}d\tau,\quad \mathbf{f}_0 = \int_0^{2\pi}\mathbf{S}^T\overline{\mathbf{f}}_0d\tau,\quad \mathbf{Q} = \int_0^{2\pi}\mathbf{S}^T\overline{\mathbf{Q}}d\tau,\quad \mathbf{P} = \int_0^{2\pi}\mathbf{S}^T\overline{\mathbf{P}}d\tau
\end{aligned}$$

Equation (13) is solved in an iterative way by using the standard Newton-Raphson iteration.

For the autonomous systems considered here, the frequency of vibration is unknown and $\Delta\omega$ is a variable to be determined. The number of knowns is greater than the number of equations by tow. This issue is dealt by seeking a solution at fixed system parameter, ie $\Delta\lambda = 0$ and enforcing one component of vector $\Delta\mathbf{A}$ equal to 0 during the iteration.

$$\mathbf{K}_{mc}\Delta\mathbf{A} = \mathbf{R} - \mathbf{R}_{mc}\Delta\omega \tag{14}$$

2.2. IHB for SDOF Van der Pol oscillator

The previously formulated IHB method for general DDE is firstly applied to a canonical Single-DOF(SDOF) delayed Van der Pol oscillator [11], which is given as

$$\ddot{y}(t) - \varepsilon\left(1 - y(t)^2\right)\dot{y}(t) + y(t) = \varepsilon k y(t - t_d) \tag{15}$$

Equation (14) in this case is reified into

$$\begin{aligned}
&\mathbf{K}_{mc} = {\omega_0}^2\mathbf{M}+\omega_0\mathbf{C} + \mathbf{C}_3+\mathbf{K} + \mathbf{K}_2+\mathbf{E}\\
&\mathbf{R} = -(\omega_0^2\mathbf{M}+\omega_0\mathbf{C} + \mathbf{K} + \mathbf{E})\mathbf{A} - \mathbf{f}_0\\
&\mathbf{R}_{mc} = (2\omega_0\mathbf{M} + \mathbf{C})\mathbf{A}+\mathbf{Q}
\end{aligned} \tag{16}$$

in which

$$\begin{aligned}
&\mathbf{M} = \int_0^{2\pi}\mathbf{S}^T\ddot{\mathbf{S}}d\tau,\quad \mathbf{C} = -\varepsilon\int_0^{2\pi}\mathbf{S}^T\dot{\mathbf{S}}d\tau,\quad \mathbf{C}_3 = \varepsilon\omega_0\int_0^{2\pi}\mathbf{S}^T(\mathbf{SA})^2\dot{\mathbf{S}}d\tau,\\
&\mathbf{K} = \int_0^{2\pi}\mathbf{S}^T\mathbf{S}d\tau,\quad \mathbf{K}_2 = 2\varepsilon\omega_0\int_0^{2\pi}\mathbf{S}^T(\dot{\mathbf{S}}\mathbf{A})(\mathbf{SA})\mathbf{S}d\tau,\quad \mathbf{E} = -\varepsilon k\int_0^{2\pi}\mathbf{S}^T\mathbf{S}\boldsymbol{\Gamma}d\tau,\\
&\mathbf{f}_0 = \varepsilon\omega_0\int_0^{2\pi}\mathbf{S}^T(\mathbf{SA})^2(\dot{\mathbf{S}}\mathbf{A})d\tau,\quad \mathbf{Q} = \varepsilon\int_0^{2\pi}\mathbf{S}^T(\mathbf{SA})^2(\dot{\mathbf{S}}\mathbf{A})d\tau
\end{aligned}$$

2.3. Cross-flow induced vibration of a tube bundle with loose supports

The second example, which is also the focus of the current study, is a practical FIV problem for a variety of industrial devices such as heat exchangers, steam generators, fluid-conveying pipes, and even transmission lines. We are interested in the FIV of a steam generator tube bundle with loose support as shown schematically in Fig. 1. As pointed out by Lever and Weaver [33,34] and other scholars, the FIV of full flexible tube bundle can be approximated by a model with a flexible tube in a rigid tube array, in particular for the problem of fluidelastic instability considered herein. The equation of motion of the elastic tube is written as

$$EI\frac{\partial^4 w}{\partial x^4} + c\frac{\partial w}{\partial t} + m\frac{\partial^2 w}{\partial t^2} + \delta(x - x_b)f(w) = F(w, \dot{w}, \ddot{w}) \tag{17}$$

where w is the lateral displacement of the beam, EI is its flexural stiffness, m is mass density, and c is the structural damping coefficient. The appearance of loose support, located at x_b from one end, gives rise to a nonlinear constraint induced force given as $f(w)\delta(x - x_b)$ with $\delta(x - x_b$ being the Dirac delta function. According to Price and Paidousiss [26], the fluidelastic force F can be expressed as

$$F(w, \dot{w}, \ddot{w}) = -\frac{\pi}{4}\rho D^2 C_{ma}\frac{\partial^2 w}{\partial t^2}(x, t) - \frac{1}{2}\rho U D C_D\frac{\partial w}{\partial t}(x, t) + \frac{1}{2}\rho U^2 D\frac{\partial C_L}{\partial w}w(x, t - \frac{D}{U}) \tag{18}$$

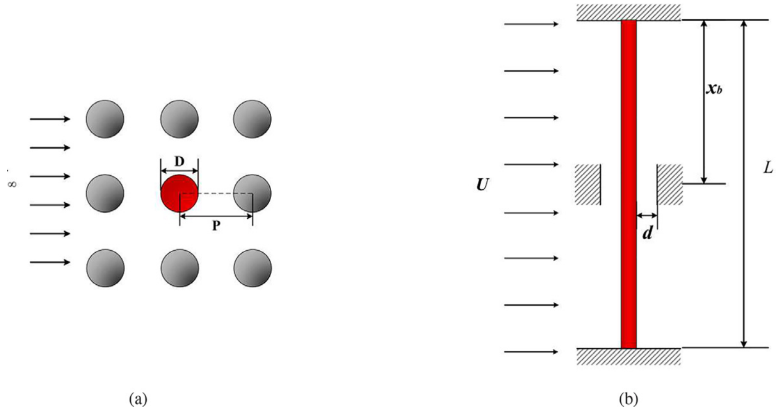

Fig. 1. Schematic of the cross-flow induced vibration of a 33 tube bundle system with loose supports, where the centred elastic tube marked in red is surrounded by rigid tubes. (a) Cross-sectional view of the tube bundle and geometric parameters. (b) Side-view of the elastic tube clamped at two ends and loosely supported at distance x_b with clearance d. (For interpretation of the references to colour in this figure legend, the reader is referred to the web version of this article.)

This is the so-called quasi-static model for fluidelastic instability of a tube array. Here, D is the diameter of the cylindrical beam, ρ and U are the fluid density and velocity, C_D and C_L are the drag and lift coefficients based on the flow velocity in the gap between the cylinders, C_{ma} is the virtual or "added" mass coefficient of the fluid around the cylinder.

It is more appropriate to recast Eq. (18) into a dimensionless form, which can be realized by introducing

$$\eta=\frac{w}{D},\qquad \xi=\frac{x}{L},\qquad \tilde{t}=\lambda_1^2\sqrt{\frac{EI}{mL^4}}t=\Omega_1 t,\qquad \zeta=\frac{c}{m\Omega_1},$$
$$\tilde{m}=\frac{m}{\rho D^2},\quad \tilde{U}=\frac{2\pi U}{D\Omega_1},\qquad \tilde{f}=\frac{f}{m\Omega_1^2},\qquad \beta=1/\left(1+\frac{4\tilde{m}}{\pi C_{ma}}\right),$$

where L is the length of the tube, and λ_1 is the dimensionless fundamental frequency of the beam. Dropping the tilde over time t, Eq. (17) may be written in the following dimensionless form

$$\frac{1}{1-\beta}\frac{\partial^2\eta}{\partial t^2}(\xi,t)+\left(\zeta+\frac{\tilde{U}C_D}{4\pi\tilde{m}}\right)\frac{\partial\eta}{\partial t}(\xi,t)+\frac{1}{\lambda_1^4}\frac{\partial^4\eta}{\partial\xi^4}(\xi,t)-\frac{\tilde{U}^2}{8\pi^2\tilde{m}}\frac{\partial C_L}{\partial\eta}\eta(\xi,t-t_d)+\delta(\xi-\xi_b)\tilde{f}(\eta)=0 \tag{19}$$

2.4. Spatial discretization by vibration modes and by finite elements

Equation (19) is a delayed nonlinear PDE. To use IHB, a spatial discretization procedure is required to convert Eq. (19) from PDE to ODEs. We use two different spatial discretization procedures, i.e. discretization via vibration modes of linear system and discretization via FEM. These two procedures share some similarities but also bear some differences. They both use basis functions for approximation, and more importantly, both involve the standard Galerkin process. The former uses vibration modes as basis functions and these basis functions are global functions and approximation is achieved via finite truncated modes. Vibration modes are concepts derived from linear vibrating system, and rigorously speaking, it is only valid for linear or weakly nonlinear systems. The basis or shape functions adopted in FEM are defined over local domains of finite elements and approximation is achieved in a local element-level. FEM discretization works well for both linear and even strongly nonlinear systems. In this sense, FEM discretization is more versatile and more accurate, but its implementation is more complicated for this FIV problem.

We firstly follow Paidoussis and Li [26] and perform spatial discretization of Eq. (19) by linear vibration modes. The modal expansion theorem is used to give

$$\eta(\xi,t)=\sum_{j=1}^{M}\phi_j(\xi)u_j(t) \tag{20}$$

in which $u_j(t)$ are the principle coordinates, M is the number of modes used for approximation, and $\phi_j(\xi)$ are the dimensionless orthonormal functions for a clamped beam, which is given as

$$\phi_j(\xi)=\cos\left(\lambda_j\xi\right)-ch\left(\lambda_j\xi\right)+\left[\sin\left(\lambda_j\xi\right)-sh\left(\lambda_j\xi\right)\right]\left(\frac{\sin\lambda_j+sh\lambda_j}{\cos\lambda_j-ch\lambda_j}\right) \tag{21}$$

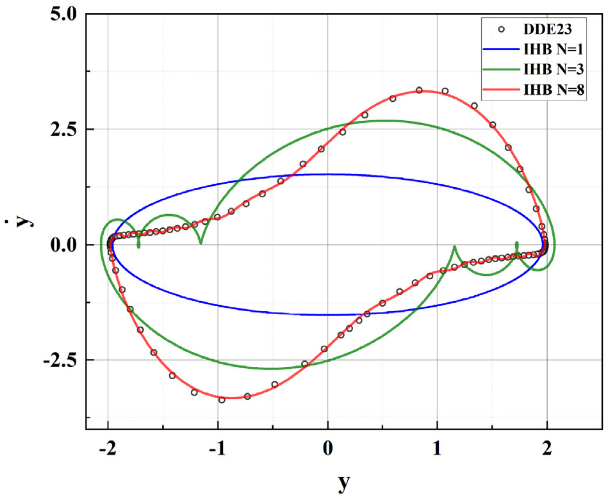

Fig. 2. The phase portraits of the delayed Van der Pol oscillator obtained by numerical integration using DDE23 function (circles) and by IHB methods using various harmonic terms (solid lines).

Since all the variables are dimensionless, we drop the tildes ($\sim$) over U, m, and f. Performing the Galerkin procedure to Eq. (19) and utilizing the orthogonality properties of the eigenfunctions, Eq. (19) can be converted into the following second-order MDOF DDEs

$$\ddot{u}_i(t) + (\alpha_1 + \alpha_2 U)\dot{u}_i(t) + \alpha_3 u_i(t) + \alpha_4 U^2 u_i(t - t_d) + (1-\beta) f(\eta_b)\phi_i(\xi_b) = 0 \qquad i = 1, 2, \ldots, M \tag{22}$$

We propose here to use combined FEM discretization and IHB method for the solution of FIV problem formulated in Eq. (19). We use C^1 elements and Hermite shape functions for approximation. A straight beam shown in Fig. 1 was discretized into a number of nodes and elements, each node having two DOFs, i.e., deflection and rotation. A corresponding weak form to Eq. (19) was constructed, and a routine Galerkin procedure yields discretized equations in the matrix forms as

$$\mathbf{M}\ddot{\delta} + \mathbf{C}\dot{\delta} + \mathbf{K}\delta + \mathbf{E}\delta(\mathbf{t}-\mathbf{t_d}) = \mathbf{f} \tag{23}$$

where **M**, **C**, **K** are the global mass, damping and stiffness matrices, respectively; **E** is the coefficient matrix of time-delay loading; **f** is impact loading force vector. Noted that the biggest contrast to mechanical vibration problems is that global mass, damping and stiffness in Eq. (23) incorporate the added mass, damping and stiffness contributions due to fluid-structure interaction. The global matrices in Eq. (23) can be obtained via a standard assemblying process in FEM. The element mass, damping and stiffness matrices, $\mathbf{M^e}$, $\mathbf{C^e}$, $\mathbf{K^e}$, as well as element time-delay loading matrix $\mathbf{E^e}$ and the element load vector $\mathbf{f^e}$ are defined as follows

$$\begin{aligned} &\mathbf{M^e} = \int_0^l \mathbf{N^T N} d\xi, \quad \mathbf{C^e} = (\alpha_1 + \alpha_2 U)\int_0^l \mathbf{N^T N} d\xi, \quad \mathbf{K^e} = \alpha_3 \int_0^l (\mathbf{N''})^\mathbf{T} \mathbf{N''} d\xi, \\ &\mathbf{E^e} = \alpha_4 U^2 \int_0^l \mathbf{N^T N} d\xi, \qquad \mathbf{f^e} = -(1-\beta)\int_0^l \delta(\xi - \xi_b) f \mathbf{N^T} d\xi \end{aligned} \tag{24}$$

where l is the length of per element in dimensionless form. Based on the Hermite shape functions for C^1 beam elements, the explicit expressions for these element matrices and vectors are given in the Appendix.

3. Results and discussions

3.1. A delay Van der Pol oscillator

We start from a SDOF delayed Van der Pol oscillator to demonstrate the effectiveness of IHB for periodic limit cycle solution. The equation of motion is given in Eq. (15). This is a second-order DDE with constant time delay t_d. The parameters of Eq. (15) are fixed as $\varepsilon = 2$, $t_d = 0.2$ and $k = 0.2$. We performed numerical integration using the MATLAB built-in solver DDE23 from an arbitrary initial condition. After a period of transient, the system approaches the periodic limit cycle, which is marked by circles in Figure.2. The solution given by DDE23 thus works as a reference solution to check the accuracy of IHB with various harmonic terms. As mentioned previously, the biggest advantage of IHB over conventional HB method lies in the fact that it is readily to incorporated more harmonic terms in approximation. Here, the number of harmonic terms, N, was set to 1,3 and 8, and the results are plotted as solid lines in Fig. 2 in comparison with DDE results. The results are inspiring, since it is very cumbersome for HB method with 8 harmonic terms. Though the system is simple, a multi-harmonic analysis is inescapable and the difference between IHB and DDE is negligible until the number of harmonic terms

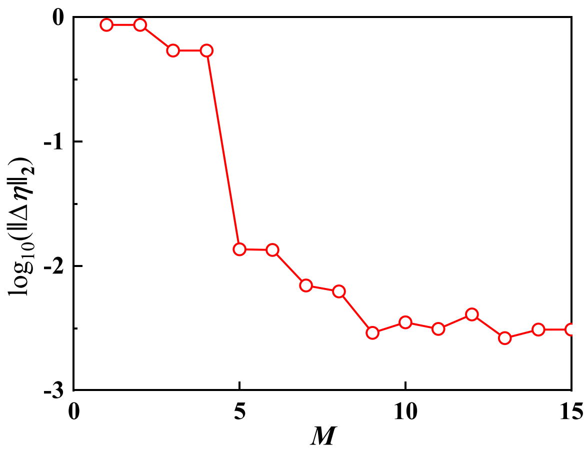

Fig. 3. Convergence of the logarithm of the L_2-norm of solution errors with increasing number of truncated vibration modes for a high gap velocity $U = 4.0$.

is increased to $N = 8$. In doing so, the derivation and code do not change, only more initial guesses for iterations are needed. In sharp contrast to IHB, all the equations and codes are written anew in the framework of HB method.

3.2. Vibration modes discretization and IHB for FIV of a loosely supported tube bundle

Figure 1 sketches the problem of interest in this paper. Without loss of generality, a square 33 tube array with pitch ratio P and tube diameter D, is chosen as the example here, which was previously studied by Paidoussis and Li [26] using NI method. We revisit this problem but instead use IHB method. The tube array is subjected to uniform cross-flow with free steam velocity U_∞. Simplifying a bundle of fully tubes into a model of a single flexible tube in a rigid array for fluidelastic instability of tube bundles is widely accepted and the simplification is adopted here. The single flexible tube is marked in red and centred in the tube array. The flexible tube is modelled as a beam with two ends clamped. A loose support with clearance d is located x_b from the end. The total beam length L and the gap velocity U used in the following discussion are also indicated on the right of Fig. 1. The gap velocity U and the free stream velocity U_∞ is related via $U = U_\infty P/(P-D)$.

The equation of vibration of a transversely loaded beam with loose support at location x_b is given by Eq. (17). The form of the equation is similar to the vibro-impact equation in non-smooth dynamics of mechanical systems, with the only exception of mechanical excitation replaced by a fluidelastic Force F with time delay. The partial differential non-dimensional beam vibration equation can be converted into ordinary differential equation by using mode summation and then employing a standard Galerkin procedure as mentioned before. The DOF of the resultant DDE in Eq. (22) is determined by the number of normal modes used for approximation. The problem considered here is complicated in nature, due not only to the complexity of fluidelastic force but also to the nonlinear boundary conditions. The complexity of the problem entails addition of more normal modes to approximate the tube displacement.

It is necessary to check convergence of the results with respect to the number of truncated modes. We use the L_2 norm measured over one period to evaluate the solution error, which is defined as

$$\|\Delta\eta\|_2 = \left\|\eta, \eta_{ref}\right\|_2 = \sqrt{\sum_{k=1}^{n}\left(\eta_k - \eta_{ref,k}\right)^2} \tag{25}$$

Here, η is the dimensionless displacement defined in Eq. (20); η_{ref} is the solution obtained by high enough order truncated modes, $M = 15$ used here; n is the number of equally spaced sampling points in one period to calculate the norm. We performed a series convergence studies to evaluate the influence of the number of truncated modes on the solution errors, and found that the required truncated modes for a convergent approximation heavily depend on gap velocity: lower order modes would give convergent solution for low velocity, whereas higher order modes are required for high velocity. This is ought to be the case since the complexity of limit cycle increases with increasing velocity. Figure 3 plots logarithmic of L_2 norm error versus truncated modes for the case $U = 4.0$, a pretty high velocity of interest here. Figure 3 indicates that five modes are sufficient to guarantee consistent solutions for all velocities considered here, and we thus fix $M = 5$ in all following examples. Our convergence study result agrees well with the observations by Paidoussis and Li [26].

Adopting five truncated modes as discussed above, the resultant 5DOF DDE in Eq. (22) is expressed in terms of principle coordinates $u_i (i = 1, 2, 3, 4, 5)$. The following coefficients in Eq. (22) were adopted for a square array with pitch ratio 1.5 [26]: $\alpha_1 = 0.0145\nu_i$, $\alpha_2 = 0.00524$, $\alpha_3 = 0.76\nu_i^2$, $\alpha_4 = 0.026$, $\beta = 0.24$, $t_d = 2\pi/U$; and $\nu_i = (\lambda_1/\lambda_i)^2$ is the square of the ratio of the ith order natural frequency to the first order natural frequency. A particular emphasis is paid to the displacement of the location where loose support appears, i.e. the displacement at $\xi = \xi_b$, which is denoted by η_b. There are several models to approximate the constraint force given by the loose support. We take the simplest assumption that the constraint force can

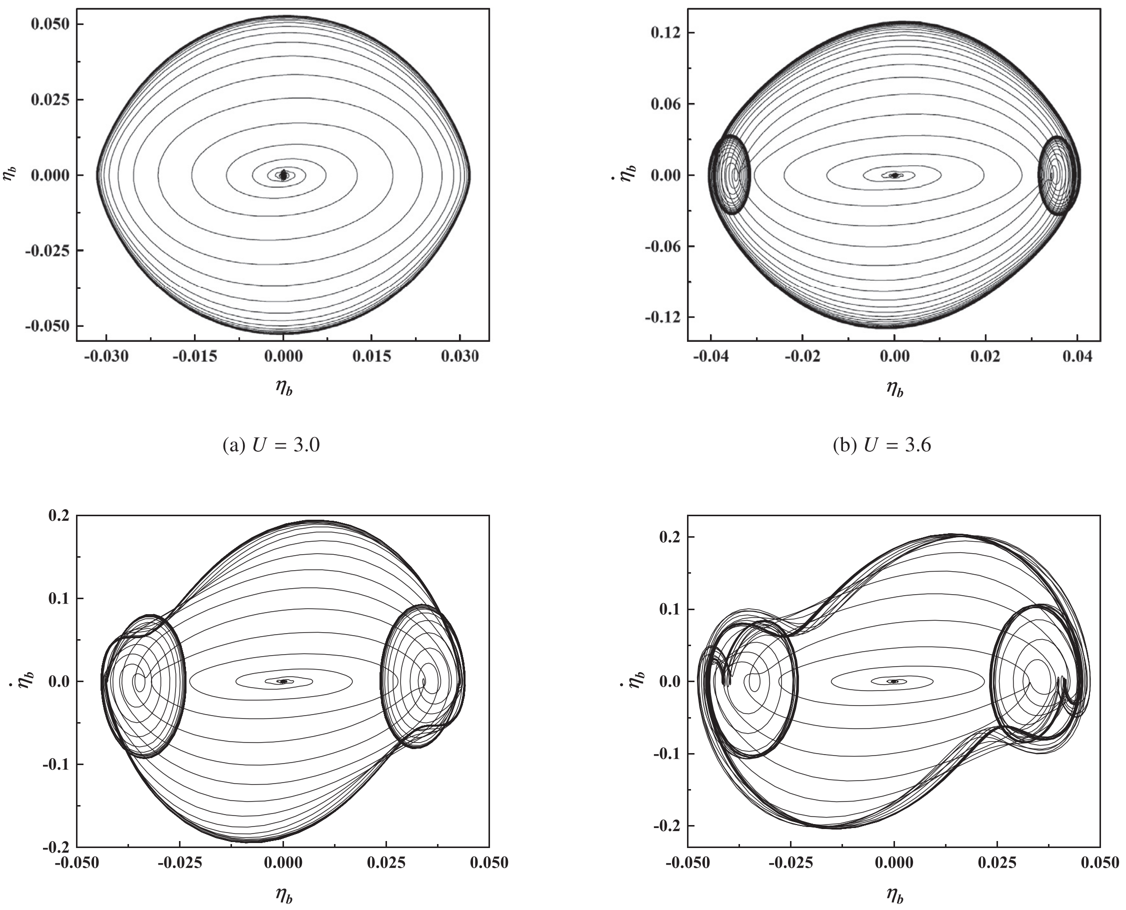

(a) $U = 3.0$ (b) $U = 3.6$

(c) $U = 4.0$ (d) $U = 4.3$

Fig. 4. The formation of limit cycles for a high-dimensional FIV system under various dimensionless gap velocities (U) 3.0 (a), 3.6 (b), 4.0 (c) and 4.3 (d), respectively. The system starts from chosen initial conditions, evolves over a long period of transient, and finally reaches periodic orbits. The whole transient process is calculated by DDE23.

be approximated by a cubic spring as $f(\eta_b) = \kappa {\eta_b}^3$, where κ is a constant taken as 1000 in accordance with Paidoussis and Li [26]. In state space, Eq. (22) is transformed into a set of high-dimensional DDEs with 10 equations.

It is not a trivial task to obtain the periodic solutions of this high-dimensional DDE. The existence of periodic limit cycles is the first thing should be considered. To this end, we employ NI using DDE23 to explore the whole dynamics of the system. Figure 4 plots the evolution of the system from arbitrary initial conditions and finally reaches limit cycles after a long period of transients. The velocities considered here are relatively high, $U = 3.0$, 3.6, 4.0 and 4.3 in Fig. 4, to guarantee the existence of limit cycles.

As unveiled by Paidoussis and Li [26], the FIV system of steam generator tube bundles with loose supports may exhibit complicated nonlinear dynamics, and the existence of periodic limit cycles does not occur for all possible gap velocities. Instead, limit cycles can only exist at an intermediate velocity. There exist two critical velocities, a low critical velocity for the onset of fluidelastic instability and a high velocity for the occurrence of quasi-periodic or even chaotic solutions. Below the low critical velocity, the system is stable and convergent to equilibrium upon any perturbations; greater than the high critical velocity, the response of the system is aperiodic. The IHB formulation presented here can only capture periodic solutions, we are thus concerned with the intermediate velocity between the two critical velocities. Actually, this part of study is the most important aspect of nonlinear time-domain models. The onset of fluidelastic instability and the corresponding critical velocity can be determined by a linear stability analysis within the framework of frequency-domain models. Chaos of tube bundles would occur at very rare high velocity, and therefore its academic significance is greater than practical importance.

We believe in the most important contribution of the paper is the introduction of IHB into cross-flow induced FIV problems of elastic tubes. We propose to replace NI by IHB for retaining limit cycle solutions. Though IHB has been developed to calculate periodic solutions of mechanical vibrating systems, this is very the first attempt to use IHB for nonlinear FIV

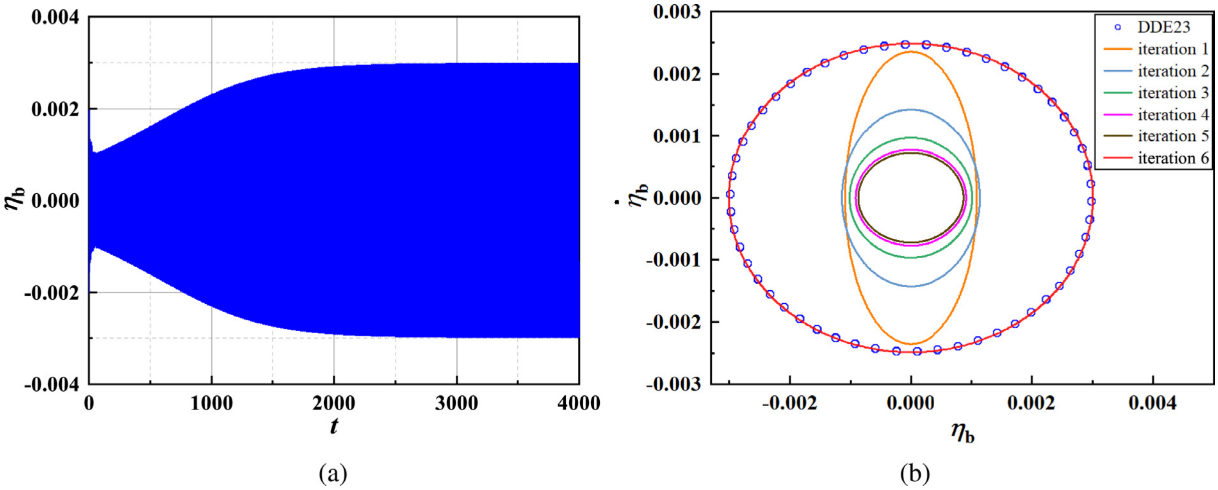

Fig. 5. Comparison of NI and IHB for obtaining limit cycle solutions of the system at a velocity, $U = 1.8$, slightly above the critical velocity $U_c = 1.78$. The displacement η_b and velocity $\dot{\eta}_b$ are evaluated at the midpoint of the beam. (a) Time history and the long period of transient process undergone by the system by using NI method (DDE23 in Matlab). (b) Evolution of limit cycle solutions (solid lines) by IHB method starting from the same initial conditions as (a). IHB solutions converge to the steady-state limit cycle in (a) (circles denoted by DDE23) after 6 iterations.

problems. The unique feature of the FIV of tube bundles lies in the fact that the interaction between the moving fluid and the vibrating tubes results in added damping and stiffness. For the damping-controlled instability concerned here, the overall damping of the system is determined by the summation of the positive structural damping and the negative fluidelastic damping. The velocities considered in Fig. 4, $U = 3.0, 3.6, 4.0$ and 4.3, are pretty larger than the critical velocity $U_c = 1.78$. For this case, the overall damping is rather negative and the equilibrium point is unstable. The nonlinearity of the system tends to restrain the unstable motion of the system from diverging, resulting in periodic or chaotic vibrations with finite amplitudes in most real applications. For this case with relatively high velocity, the convergence of transient solution starting from an arbitrarily chosen initial conditions to the steady limit cycles is rather slow but still acceptable. It seems that the advantage of using IHB rather than NI is not so obvious. The situation changes dramatically as one decreases gap velocity to a value slightly above U_c, say $U = 1.8$. Figure 5 shows the comparison between NI using DDE23 and IHB for limit cycle solutions at $U = 1.8$, all starting from the same initial conditions. In this case, the overall damping is very close to zero, and the convergence of the transient to limit cycles is extremely slow and unacceptable if NI method is used. In this study, a personal computer with a CPU of 11th Gen Intel(R) Core(TM) i5-11300H @ 3.10GHz and 16 G RAM was used, and 115 s were needed to retain the steady-state limit cycle solutions using the DDE23 function in Matlab. As a sharp contrast, the iteration of IHB method started from an initial guess of a limit cycle solution and efficiently converged to the final solution after 6 iterations, which took 3 s in calculation. Both NI and IHB adopt the same arbitrary initial conditions. The advantage of replacing NI by IHB for limit cycles of FIV systems manifests itself through this example.

Figure 6 plots and compares limit cycle solutions obtained by NI using DDE23 and by IHB using different harmonic terms. As described above, the velocities of interest are $U = 3.0$, 3.6, 4.0 and 4.3, respectively. The critical velocity for the onset of fluidelastic instability is about $U_c = 1.78$, whereas the high critical velocity for the occurrence of chaos is about 4.39. Figure 6 indicates that the complexity of nonlinear dynamics of the system increases as the dimensionless gap velocity increases. At low gap velocity, i.e. $U = 3.0$ in Fig. 6(a), the shape of the limit cycle is simple, nearly an ellipse in this case. Focusing on the middle point of the beam where loose support is located, in Fig. 6(a) the limit cycle passes the extremes of displacement twice, where the velocity $\dot{\eta}_b$ is zero, for the case $U = 3.0$. For this case with simple limit cycle, one harmonic term approximation with $N = 1$ in Fig. 6(a) can nearly capture the periodic solution, and the solutions with $N = 3$ and 5 give the identical solution as given by DDE23. As velocity increases to 3.6 and 4.0 in Fig. 6(b) and (c), the complexity of limit cycles increases, passing the positions marked by $\dot{\eta}_b = 0$ six times with nested cycles. The single harmonic IHB can only give a simple limit cycle and there is no way to capture this nested cycles phenomenon. Though IHB with three harmonic terms capture this phenomenon, the difference between IHB with $N = 3$ and DDE23 is obvious. IHB with five harmonic terms is necessary for this two cases, and the IHB can give the same results as DDE23. If the velocity is further increased to $U = 4.3$ as shown in Fig. 6(d), the complexity of limit cycle increases further, passing the positions with $\dot{\eta}_b = 0$ ten times. For this case, IHB with $N = 5$ can also capture the complicated limit cycles.

Figure 4 and 6 are plotted for a set of fixed gap velocities. They also imply the fact that gap velocity is a key system parameter that controls the nonlinear dynamics of the system. We finally demonstrate the merit of IHB for large range parametric study. The results are plotted in Fig. 7 for amplitudes A and frequencies of limit cycles f versus various dimensionless gap velocities U. Figure 7 shows that both amplitude and frequency of limit cycles increase monotonically with increasing velocity, and it seems that both reach stationary values at high velocities. In IHB method, performing the parametric study

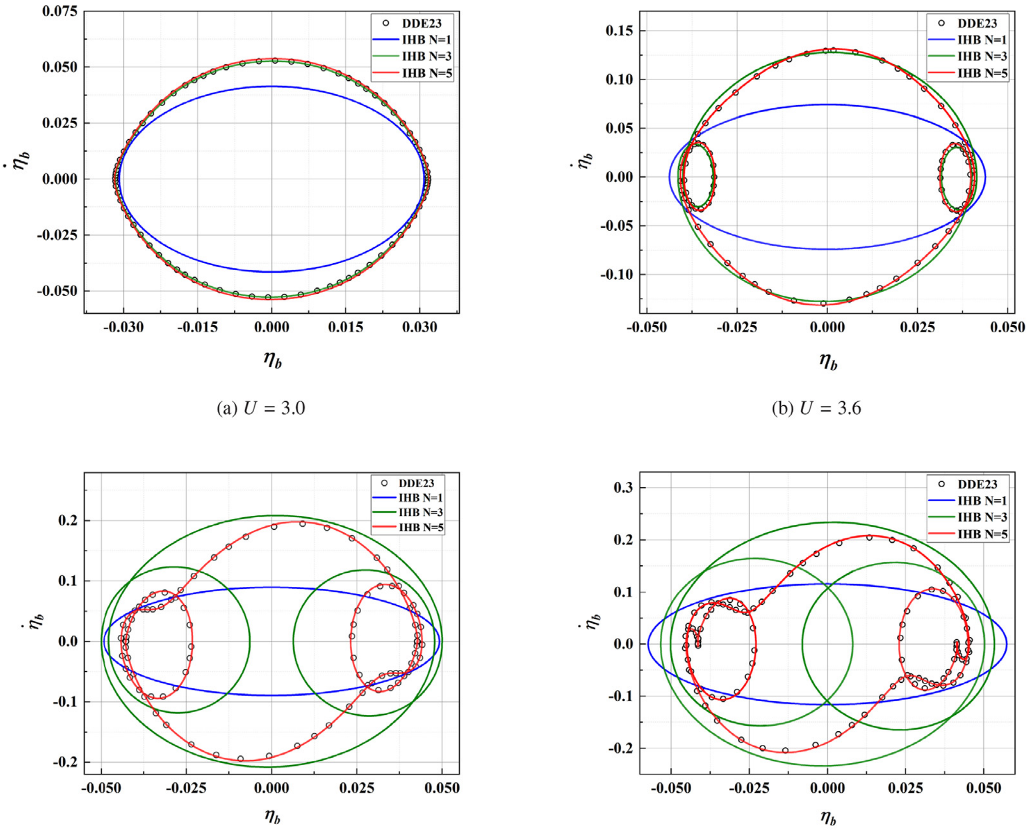

(a) U = 3.0

(b) U = 3.6

(c) U = 4.0

(d) U = 4.3

Fig. 6. Comparison of limit cycles obtained by numerical integration using DDE23 function (circles) and by IHB with different harmonic terms (solid lines).

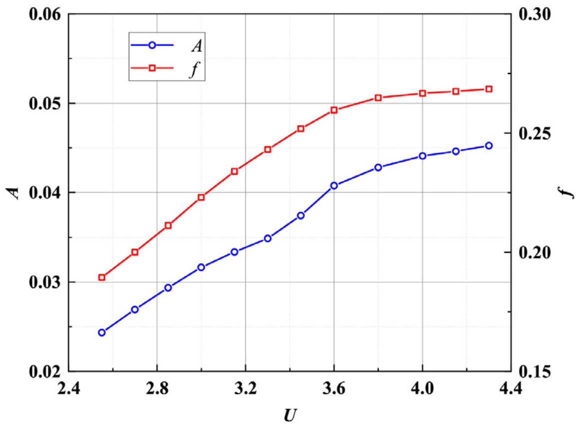

Fig. 7. Variation of amplitudes and frequencies with dimensionless gap velocity U.

in Fig. 7 is straightforward, because the formulation incorporates system parameter and the parameter can be augmented in an incremental manner. The unique feature of tuning parameter makes IHB flexible and straightforward for large range parametric analysis.

3.3. Combined FEM and IHB for FIV of tube bundles

All the afore-mentioned IHB results are based on spatial discretization using vibration modes. Since the problem considered here is nonlinear in nature, to what extent does the mode summation method work well remains a plausible question.

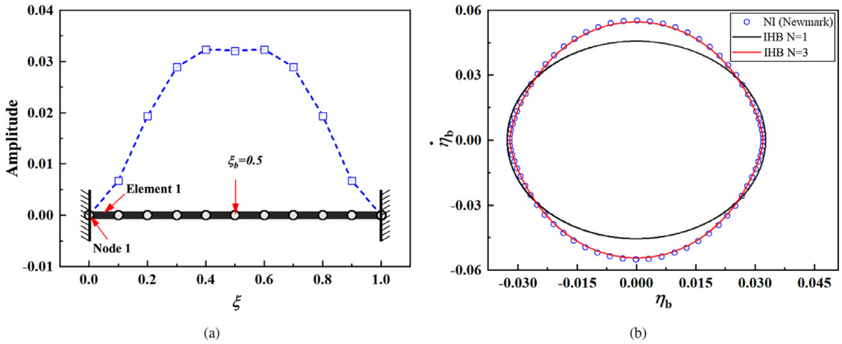

Fig. 8. Combination of FEM with IHB for the analysis of FIV of a 10-element beam problem. (a) The FEM model (black solid line and filled circles) and the limit cycle amplitudes extracted from various nodes of FEM model (blue dashed line and filled squares). (b) Comparison of IHB solutions with N =1 and 3 (solid lines) and NI solution (circles) by Newmark method. (For interpretation of the references to colour in this figure legend, the reader is referred to the web version of this article.)

Here we propose to use combined FEM discretization and IHB iteration to this nonlinear FIV problem. FEM works well for either linear or nonlinear systems, thus the solution by combination of FEM and IHB could be regarded as the solution of original problem, as opposed to the previously approximate truncated systems. We implemented the formulations given in Section 2. The straight beam subjected to uniform cross-flow was discretized by 10 C^1 beam elements. The dimensionless length of each element was set to 0.1. The coefficients in Eq. (24) are the same as those of Eq. (22) except that $\alpha_1 = 0.0145$, $\alpha_3 = 0.00152$. Figure 8(a) shows the illustration of the FEM model and boundary conditions. Each node has two independent DOFs, i.e., deflection and rotation. 9 nodes are free to vibrate accounting for boundary conditions, and therefore the discretized equation in Eq. (23) contains 18 DOF second-order DDEs, which is really a high-dimensional system. We obtained periodic solutions of all 9 nodes, and Fig. 8(a) plots the spatial variation of defection amplitudes of the nodes. The amplitude distribution for rotation of the nodes can be obtained in the same way.

The IHB solution of the 18DOF DDEs with multiple harmonics requires a large number of initial values of harmonic coefficients. If three harmonics are included, i.e., $N = 3$, then totally 118 initial guesses are needed, which constitutes an issue for IHB implementation. In practice, we firstly achieved an approximate solution containing only single harmonics, and the solution for $N = 1$ was used as initial guesses for $N = 3$. Figure 8(b) plots the convergence of IHB solutions starting from limit cycle for $N = 1$ to the cycle for $N = 3$.A comparison is made between IHB solution with the NI solution. It should be emphasized that the built-in routine DDE23 in Matlab runs highly slowly for such an 18DOF DDE system, and a recourse was made to programme other efficient algorithms for NI of DDE. This was realized by coding a Newmark NI code tailored for DDE, and we found the saving of computation is significant.

4. Concluding remarks

DDEs govern a variety of science and engineering problems, in which conventional ODEs in principle fail to describe these systems. The appearance of time-delay or the aftereffect entails more expensive numerical procedures or more delicate treatment. For a nonlinear DDE, the periodic solution is the most important aspect of the nonlinear dynamics, and great efforts have been made to calculate the periodic solutions of nonlinear DDE. Among various methods for periodic solutions of DDEs, the extension of classical HB to IHB is worth attention because of several unique features of IHB: it does not limit to weak nonlinearity; it can capture not only stable but also unstable solutions; it is more straightforward to perform multi-harmonic analysis, and it is well suitable for large range parametric analysis.

To date, there have been a few of studies which develop or extend IHB to find periodic solutions of DDEs. But these previous studies are limited to low-dimensional mechanical vibration systems. This paper introduces the IHB method into the limit cycle solution of flow-induced vibration problem of tube bundles with loose support. FIV of tube bundle is a unique system in the sense that the added damping cancels out structural damping in the vicinity of critical velocity, making it extremely slow to retain a convergent solution if numerical integration (NI) is utilized. Thus the replacement of NI by IHB is desperately needed under such a condition. To the best knowledge of the authors, no efforts have been made to employ IHB for nonlinear FIV problems. This paper describes the IHB formulations of general MDOF DDE with various discrete time-delays. We separately implement two spatial discretization strategies, i.e., discretization via linear vibration modes and via finite element method (FEM), and combine the spatial discretization with IHB formulation to capture limit cycle solutions after the onset of instability. For high gap velocity, the system may exhibit complicated periodic solutions, and a multi-harmonic analyses are required to accurately approximate the solution. We compare the solutions obtained by NI method and by IHB with various harmonic terms. The comparison demonstrates excellent convergence of IHB to exact solution by increasing harmonic terms for approximation. The FIV system was investigated for various gap velocities, and IHB works well not only for low velocity but also for high gap velocities where the phase portraits have complicated nested cycles. We show that IHB is an ideal tool for calculating amplitudes and frequencies of limit cycles for a wide range of gap velocity variation.

The integration of FEM discretization with IHB is an appealing approach. It overcomes the limitation of previously used vibration mode discretization and then time-marching strategy for nonlinear FIV problems. It is not limited to linear or weakly nonlinear systems, and is an ideal candidate for FIV systems with complicated geometries, where vibration modes are not readily available and could not be given in close forms. This is crucial for steam generators with U-tubes or helical tubes. A straight beam subjected to uniform cross-flow is studied here, and a 10-element discretization gives to a high-dimensional 18DOF DDE system. Increasing the IHB harmonic terms from one to three demonstrates excellent convergent property, and good agreement is achieved between IHB results and results by a tailored Newmark NI method for DDE. Our efforts provide the first reference on the use of IHB for high-dimensional FIV problems with time-delays, which opens an avenue for efficient multi-harmonic analysis of high-dimensional DDE due to the semi-analytical feature of IHB.

Data availability

Data will be made available on request.

Acknowledgment

This research is supported by National Natural Science Foundation of China (grant 11972277) and by Science and Technology on Reactor System Design Technology Laboratory (LRSDT2021205).

Appendix A

$\mathbf{K}_{mc}$, $\mathbf{R}$, $\mathbf{R}_{mc}$, in Vibration modes discretization method of the FIV system, should obey the following form:

$$\begin{aligned}
&\mathbf{K}_{mc} = {\omega_0}^2\mathbf{M}+\omega_0\mathbf{C}+\mathbf{K}+\mathbf{K}_3+\mathbf{E}\\
&\mathbf{R} = -(\omega_0^2\mathbf{M}+\omega_0\mathbf{C}+\mathbf{K}+\mathbf{E})\mathbf{A}-\mathbf{f}_0\\
&\mathbf{R}_{mc} = (2\omega_0\mathbf{M}+\mathbf{C})\mathbf{A}
\end{aligned}\tag{A.1}$$

in which

$$\mathbf{M} = \int_0^{2\pi}\mathbf{S}^T\overline{\mathbf{M}}\dot{\mathbf{S}}d\tau,\quad \mathbf{C} = \int_0^{2\pi}\mathbf{S}^T\overline{\mathbf{C}}\dot{\mathbf{S}}d\tau,\quad \mathbf{K} = \int_0^{2\pi}\mathbf{S}^T\overline{\mathbf{K}}\mathbf{S}d\tau$$
$$\mathbf{K}_3 = \int_0^{2\pi}\mathbf{S}^T\overline{\mathbf{K}}_N\mathbf{S}d\tau,\quad \mathbf{E} = \int_0^{2\pi}\mathbf{S}^T\overline{\mathbf{E}}\mathbf{S}\boldsymbol{\Gamma}d\tau,\quad \mathbf{f}_0 = \int_0^{2\pi}\mathbf{S}^T\bar{\mathbf{f}}_0d\tau$$

and

$$\begin{aligned}
&\bar{\mathbf{M}} = diag\left\{1,\quad 1,\quad 1,\quad 1,\quad 1\right\}\\
&\bar{\mathbf{C}} = diag\left\{\alpha_1(1)+\alpha_2U,\quad \alpha_1(2)+\alpha_2U,\quad \alpha_1(3)+\alpha_2U,\quad \alpha_1(4)+\alpha_2U,\quad \alpha_1(5)+\alpha_2U\right\}\\
&\bar{\mathbf{K}} = diag\left\{\alpha_3(1),\quad \alpha_3(2),\quad \alpha_3(3),\quad \alpha_3(4),\quad \alpha_3(5)\right\}\\
&\bar{\mathbf{K}}_3 = 3(1-\beta)\kappa{\eta_b}^2diag\left\{[\phi_1(\xi_b)]^2,\quad [\phi_2(\xi_b)]^2,\quad [\phi_3(\xi_b)]^2,\quad [\phi_4(\xi_b)]^2,\quad [\phi_5(\xi_b)]^2\right\}\\
&\bar{\mathbf{E}} = diag\left\{\alpha_4U^2,\quad \alpha_4U^2,\quad \alpha_4U^2,\quad \alpha_4U^2,\quad \alpha_4U^2\right\}\\
&\bar{\mathbf{f}}_0 = (1-\beta)\kappa{\eta_b}^3diag\left\{\phi_1(\xi_b),\quad \phi_2(\xi_b),\quad \phi_3(\xi_b),\quad \phi_4(\xi_b),\quad \phi_5(\xi_b)\right\}
\end{aligned}$$

The explicit expressions for element matrices $\mathbf{M^e}$, $\mathbf{C^e}$, $\mathbf{K^e}$ and $\mathbf{E^e}$ in FEM model are given as follows:

$$\begin{aligned}
&\mathbf{M^e} = \frac{l}{420}\begin{bmatrix}156 & 22l & 54 & -13l\\ 22l & 4l^2 & 13l & -3l^2\\ 54 & 13l & 156 & -22l\\ -13l & -3l^2 & -22l & 4l^2\end{bmatrix},\qquad \mathbf{C^e} = \frac{l(\alpha_1+\alpha_2U)}{420}\begin{bmatrix}156 & 22l & 54 & -13l\\ 22l & 4l^2 & 13l & -3l^2\\ 54 & 13l & 156 & -22l\\ -13l & -3l^2 & -22l & 4l^2\end{bmatrix},\\
&\mathbf{K^e} = \frac{\alpha_3}{l^3}\begin{bmatrix}12 & 6l & -12 & 6l\\ 6l & 4l^2 & -6l & 2l^2\\ -12 & -6l & 12 & -6l\\ 6l & 2l^2 & -6l & 4l^2\end{bmatrix},\qquad \mathbf{E^e} = \frac{l\alpha_4U^2}{420}\begin{bmatrix}156 & 22l & 54 & -13l\\ 22l & 4l^2 & 13l & -3l^2\\ 54 & 13l & 156 & -22l\\ -13l & -3l^2 & -22l & 4l^2\end{bmatrix}
\end{aligned}\tag{A.2}$$

References

[1] V. Kolmanovskii, A. Myshkis, Introduction to the Theory and Applications of Functional Differential Equations, Vol. 463, Springer Science & Business Media, 2013.
[2] R.D. Driver, Ordinary and Delay Differential Equations, Vol. 20, Springer Science & Business Media, 2012.
[3] A. Bellen, M. Zennaro, Numerical Methods for Delay Differential Equations, Oxford University Press, 2013.
[4] J.-P. Richard, Time-delay systems: an overview of some recent advances and open problems, Automatica 39 (10) (2003) 1667–1694.
[5] K. Engelborghs, V. Lemaire, J. Belair, D. Roose, Numerical bifurcation analysis of delay differential equations arising from physiological modeling, J. Math. Biol. 42 (4) (2001) 361–385.
[6] J. Sieber, K. Engelborghs, T. Luzyanina, G. Samaey, D. Roose, DDE-BIFTOOL manual-bifurcation analysis of delay differential equations, arXiv preprint arXiv:1406.7144 (2014).
[7] D. Pieroux, P. Mandel, Bifurcation diagram of a complex delay-differential equation with cubic nonlinearity, Phys. Rev. E Stat. Nonlin. Soft Matter Phys. 67 (5 Pt 2) (2003) 056213.
[8] D. Roose, R. Szalai, Continuation and bifurcation analysis of delay differential equations, Numer. Continuation Methods Dyn.Syst. (2007) 359–399.
[9] N. MacDonald, Harmonic balance in delay-differential equations, J. Sound Vib. 186 (4) (1995) 649–656.
[10] L. Liu, T. Kalmár-Nagy, High-dimensional harmonic balance analysis for second-order delay-differential equations, J. Vib. Control 16 (7–8) (2010) 1189–1208.
[11] L. Guillot, C. Vergez, B. Cochelin, Continuation of periodic solutions of various types of delay differential equations using asymptotic numerical method and harmonic balance method, Nonlinear Dyn. 97 (1) (2019) 123–134.
[12] X. Wang, W. Zhu, X. Zhao, An incremental harmonic balance method with a general formula of jacobian matrix and a direct construction method in stability analysis of periodic responses of general nonlinear delay differential equations, J. Appl. Mech. 86 (6) (2019). 061011–1
[13] M. Song, W. Zhu, Elastic wave propagation in strongly nonlinear lattices and its active control, J. Appl. Mech. 88 (7) (2021) 071003.
[14] R. Mitra, A. Banik, S. Chatterjee, Response of a harmonically forced dry friction damped system under time-delayed state feedback, J. Comput. Nonlinear Dyn. 13 (3) (2018). 031001–1
[15] Z. Liu, K. Hu, K.-w. Chung, Nonlinear analysis of a closed-loop tractor-semitrailer vehicle system with time delay, Mech. Syst. Signal Process. 76 (2016) 696–711.
[16] F. Shakeri, M. Dehghan, Solution of delay differential equations via a homotopy perturbation method, Math. Comput. Model. 48 (3–4) (2008) 486–498.
[17] J.-H. He, Periodic solutions and bifurcations of delay-differential equations, Phys. Lett. A 347 (4–6) (2005) 228–230.
[18] Y. Chen, J. Xu, Applications of the integral equation method to delay differential equations, Nonlinear Dyn. 73 (4) (2013) 2241–2260.
[19] A. Maccari, Vibration control for the primary resonance of the van der Pol oscillator by a time delay state feedback, Int. J. Non Linear Mech. 38 (1) (2003) 123–131.
[20] A. Maccari, The response of a parametrically excited van der Pol oscillator to a time delay state feedback, Nonlinear Dyn. 26 (2) (2001) 105–119.
[21] H. Wang, H. Hu, Bifurcation analysis of a delayed dynamic system via method of multiple scales and shooting technique, Int. J. Bifurcation Chaos 15 (02) (2005) 425–450.
[22] K. Engelborghs, T. Luzyanina, D. Roose, Numerical bifurcation analysis of delay differential equations, J. Comput. Appl. Math. 125 (1–2) (2000) 265–275.
[23] D.A. Barton, B. Krauskopf, R.E. Wilson, Collocation schemes for periodic solutions of neutral delay differential equations, J. Differ. Equ. Appl. 12 (11) (2006) 1087–1101.
[24] H. Wu, X. Zeng, Y. Liu, J. Lai, Analysis of harmonically forced duffing oscillator with time delay state feedback by incremental harmonic balance method, J. Vib. Eng. Technol. 9 (6) (2021) 1239–1251.
[25] B.W. Roberts, Low frequency, aeroelastic vibrations in a cascade of circular cylinders, Mech. Sci. Monogr. (4) (1966).
[26] M. Paidoussis, G.X. Li, Cross-flow-induced chaotic vibrations of heat-exchanger tubes impacting on loose supports, J. Sound Vib. 152 (2) (1992) 305–326.
[27] S. Lau, Y. Cheung, Amplitude incremental variational principle for nonlinear vibration of elastic systems, J. Appl. Mech. 48 (4) (1981) 959–964.
[28] S. Lau, Y. Cheung, S. Wu, Nonlinear vibration of thin elastic plates. Part I: generalized incremental Hamilton's principle and element formulation, J. Appl. Mech. 51 (4) (1984) 837–844.
[29] S. Lau, Y. Cheung, S. Wu, Nonlinear vibration of thin elastic plates. Part II: internal resonance by amplitude-incremental finite element, J. Appl. Mech. 51 (4) (1984) 845–851.
[30] Y. Cheung, S. Chen, S. Lau, Application of the incremental harmonic balance method to cubic non-linearity systems, J. Sound Vib. 140 (2) (1990) 273–286.
[31] C. Pierre, A. Ferri, E. Dowell, Multi-harmonic analysis of dry friction damped systems using an incremental harmonic balance method, J. Appl. Mech. 52 (4) (1985) 958–964.
[32] S. Lau, W.-S. Zhang, Nonlinear vibrations of piecewise-linear systems by incremental harmonic balance method, J. Appl. Mech. 59 (1) (1992) 153–160.
[33] J. Lever, D. Weaver, On the stability of heat exchanger tube bundles, Part I: modified theoretical model, J. Sound Vib. 107 (3) (1986) 375–392.
[34] J. Lever, D. Weaver, On the stability of heat exchanger tube bundles, Part II: numerical results and comparison with experiments, J. Sound Vib. 107 (3) (1986) 393–410.